Heterogeneities and material-scales providing physically-based damping to replace Rayleigh damping for any structure size

Adnan Ibrahimbegovic[*,1,2,3] and Rosa Adela Mejia Nava[1]

[1]*Universite de Technologie de Compiegne – Alliance Sorbonne Universite, 60203 Compiegne, France*
[2]*Chair of Computational Mechanics UTC*
[3]*IUF Institut Universitaire de France*

Abstract. This study is aimed to develop a damping model to accurately predict vibration amplitude reduction for any size of structure. It is developed in the framework of multi-scale analysis, where different sources of energy dissipation at captured at material-scales (e.g., scale of representative volume element). In particular, we illustrate details for concrete structures, where one needs different failure mechanisms like plasticity, damage and viscosity to represent different sources of dissipation are reproduce the typical hysteresis loops of concrete with both residual deformation and change of initial elastic response. The final step in proposed approach is to account for structure heterogeneities by allowing for variability of elasticity limit, which produces the same exponential (rather than linear decay) of vibration amplitudes, just as in the case of Rayleigh damping. However, contrary to Rayleigh damping calibration that can be done only on a single structure (and for a chosen frequency), the proposed approach can be adapted to any structure size and full interval of frequencies of interest. The price to pay is in terms of nonlinear analysis, which is here rendered very efficient by hybrid-stress formulation to uncouple different damage mechanisms and by using linear evolution equations for internal variables representing such mechanisms. The details illustrated for 1D and 3D concrete model can be easily adapted to other materials, such as steel, soils etc.

Keywords: Rayleigh damping replaced; material-scale mechanisms; probability, structure heterogeneities

1. Introduction

1.1 Preliminary remarks on what is wrong with the Rayleigh damping model for dynamics

Currently dominant approach in engineering practice when studying dynamic vibration of engineering structures or systems relies upon well-known equations of motion (e.g., Clough and Penzien 2006, Chopra 1995). For forced vibrations of an undamped system, the equations of motion for can be written in the form

$$M\ \ddot{u}(\text{t}) + K\ u(\text{t}) = f(\text{t}) \tag{1}$$

---

*Corresponding author, Professor, E-mail: adnan.ibrahimbegovic@utc.fr

where M and K are respectively structure stiffness and mass matrix, $f(t)$ is applied dynamic force (e.g., earthquake, wind, explosions etc.) and $u(t)$ is corresponding dynamic response. The main advantage of such an approach is in that allows for very efficient computations by appealing to the classical mode superposition approach (e.g., Clough and Penzien 2006, Chopra 1995, Geradin and Rixen 2015) where the equations of motion are uncoupled in terms of modal response (representing the motion of a complex structure in a particular mode of free vibrations) and solved easily, either analytically or numerically, (e.g., Ibrahimbegovic 2009) for each of these equations independently.

In order to account for damped vibrations (which certainly corresponds to reality, since the vibrations eventually stop due to different energy dissipation mechanisms), one then uses the well-known Rayleigh damping (e.g., Clough and Penzien 2006, Ibrahimbegovic and Ademovic 2019). The latter assumes that the damping phenomena are proportional to vibration velocities, with the coefficient of proportionality, so called damping matrix C, which can be constructed as linear combination of mass and stiffness matrix

$$C = a_0 \, M + a_1 \, K \tag{2}$$

where two coefficients, or Rayleigh parameters a_0 and a_1, are obtained from chosen damping coefficient ζ that characterize a typical attenuation of vibration amplitudes with typical choices of 5% for concrete and 2% for steel structures; see (Ibrahimbegovic and Ademovic 2019) on how to simply obtain the Rayleigh parameters according to:

$$\xi = a_0 / 2\omega_n \quad \text{or} \quad \xi = a_1 \omega_n / 2 \tag{3}$$

where ω_n is the chosen frequency that should be damped with precisely the chosen amount of damping. The best one can to further improve that, given two Rayleigh parameters, is to choose two different frequencies ω_n and ω_m and make sure that chosen damping coefficients would precisely apply to those two modes. However, one has to realize that all other frequencies would be damped in the way that is quite unrealistic, either somewhat less (inside the interval between chosen frequencies) or much more – see Fig. 1 for illustration (Ibrahimbegovic and Ademovic 2019).

1.2 What we propose as more material-scale-base damping model for dynamics capable of representing different phases of dynamic response
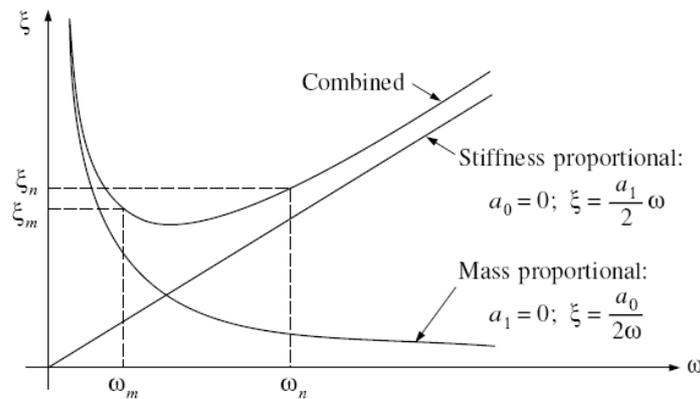
Fig. 1 Relationship between damping ratio and frequency (for Rayleigh damping) (Ibrahimbegovic and Ademovic 2019)
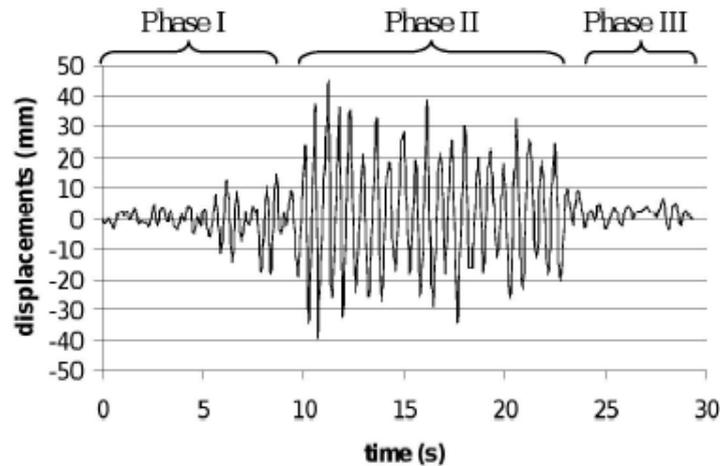
Fig. 2 Three typical phases of earthquake induced vibrations: i) small vibration amplitudes at start, ii) strong shaking with large vibration amplitudes for the dominant phase, and iii) free vibrations of damaged structure after earthquake excitation stops

What we seek to construct and develop in this paper is very new concept damping obtained from material scales, which can provide much better correlation with dynamics response of real life structures, under complex loading such as earthquake. More precisely, a very typical response to earthquake (see Fig. 2) passes through three different phases: i) small vibration amplitudes for mild earthquake, ii) strong shaking with large vibration amplitudes for the dominant phase of earthquake excitation, and iii) free vibrations of damaged structure produced once the earthquake excitation stops.

It is clear that the Rayleigh damping cannot come even close to representing these three different phases of vibration amplitudes under earthquake motion, since the damping ratio in (1) or the fit in Fig. 3 can only capture one particular frequency interval. In this paper, we present a completely different approach, where different sources of energy dissipation are presented on physically-based ground at material scales. In this manner we can indeed capture different phenomena that are triggered as we go along the earthquake excitation from mild to strong shaking to finally free vibrations of a damaged structure. This is explained for concrete structures by combining plasticity, damage and viscosity models to capture typical hysteresis loops of concrete material. The development relies upon and extends our previous works on modeling concrete structure damage mechanisms at material-scales (Ibrahimbegovic *et al*. 2008, Jehel *et al*. 2010, Karavelic *et al*. 2019). The details corresponding to development are given in Section 2.

There is yet another deficiency of the Rayleigh damping that we address and correct in this work by judicious combination of material-scale modeling and structure heterogeneities probability description (Ibrahimbegovic *et al*. 2011, Ibrahimbegovic *et al*. 2014, Ibrahimbegovic *et al*. 2021).

Namely, the identification fit we can use with the Rayleigh damping is valid only at the structural level. More precisely, once we have recorded the structure response, we ought to identify the corresponding damping leading to particular time variation of displacement (such in Fig. 2). How is this handled with Rayleigh damping? The typical dynamic response given for Rayleigh damping pertains to exponential decay of amplitudes, until final time of vibrations, with a bigger amplitude decay for larger values of damping ratio (see Fig. 3).
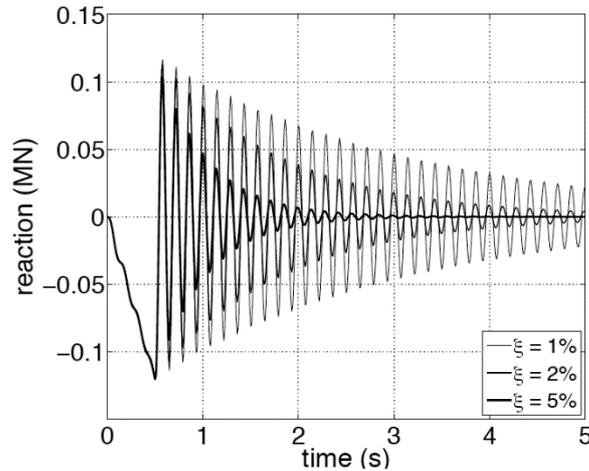
Fig. 3 Typical exponential amplitude decay for Rayleigh damping for three different values of damping ratio

The damping characteristics here are sought for a typical structural system where we express the damping of such real system in terms of equivalent viscous damping ratio that shows similar decay rates under free vibration conditions. More precisely, it is easy to obtain with the exponential amplitude decay that by considering any two successive positive peaks, such as v_n and v_{n+1}, the natural logarithm of the ratio of these two successive values is given by the so-called logarithmic decrement of damping δ (Clough and Penzien 2006)

$$\delta \equiv \ln \frac{v_n}{v_{n+1}} = \frac{2\pi\xi}{\sqrt{1 - \xi^2}} \tag{4}$$

which is often further simplified to $\delta = 2\pi\xi$ for small damping values. Hence, the experimental damping identification with Rayleigh damping is carried out for a particular structure, by measuring the logarithmic decrement of damping and thus deducing the corresponding value of damping coefficient for such structure. Needless to say, such measurement is valid only for a particular structure, and thus the standard procedure for damping identification just described is influenced by the structure size, and cannot be considered intrinsic value that can apply to any size of the structure.

We will show in Section 3 that the amplitude decay for homogeneous structure is typical of plasticity and damage sources of dissipation, which are comparable to dry friction. Namely, it was shown by Inman (2001) that the dry friction type of damping leads to linear amplitude decay. However, the key novel idea we illustrate here is the fact that by accounting for structure heterogeneities – which implies the variation of limit of elasticity at different points of the structure – we indeed recover the exponential decay typical of experimental results. Hence, we do obtain the same result as the one with the Rayleigh damping, but not by 'forcing' the type or response for a typical structure, but rather by using the intrinsic procedure from material scale and probability based extrapolation to structure scale. In this manner, we can deal with damping interpretation for structure of any size.

2. Multi-scale model of concrete in cyclic loading
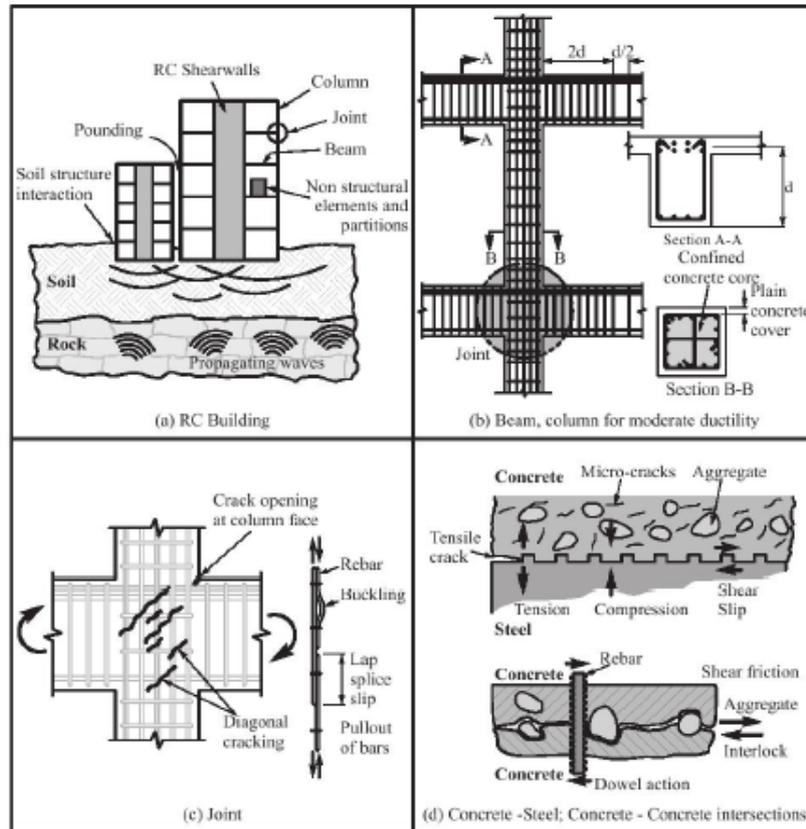
Fig. 4 Typical sources of energy dissipation under earthquake induced vibrations for concrete and reinforced-concrete structures

2.1 Material-scales basis for representing sources of energy dissipation through internal variables

Obviously the structure-level identification procedure typical of the Rayleigh damping cannot be fully representative of different sources of energy dissipation, such as illustrated in Fig. 4 for typical concrete and reinforced-concrete structure.

Given large diversity of the sources illustrated in Fig. 4, we will further focus upon the energy dissipation sources in concrete, during typical hysteresis loops in cyclic loading (see Fig. 5(a)). In order to be able to capture the energy dissipation in each hysteresis loop, we ought to use combined plasticity, damage and viscosity model (Ibrahimbegovic *et al.* 2008) to represent real response of concrete material for typical cyclic loading. In fact, we do simplify this representation somewhat, by choosing the linear evolution equations (e.g., linear hardening) so as to be able to carry out computations more efficiently. As the consequence, the hysteresis loops produced by our model (see Fig. 5(b)) will not have 'rounded' hysteresis loops typical of experimental results, but rather rhombic type of shape. However, in the identification phase (described in the next section), we will make sure that the dissipated energy in a typical cycle remains the same between experiment and the model prediction, even though the shape is not entirely the same – the area enclosed by each
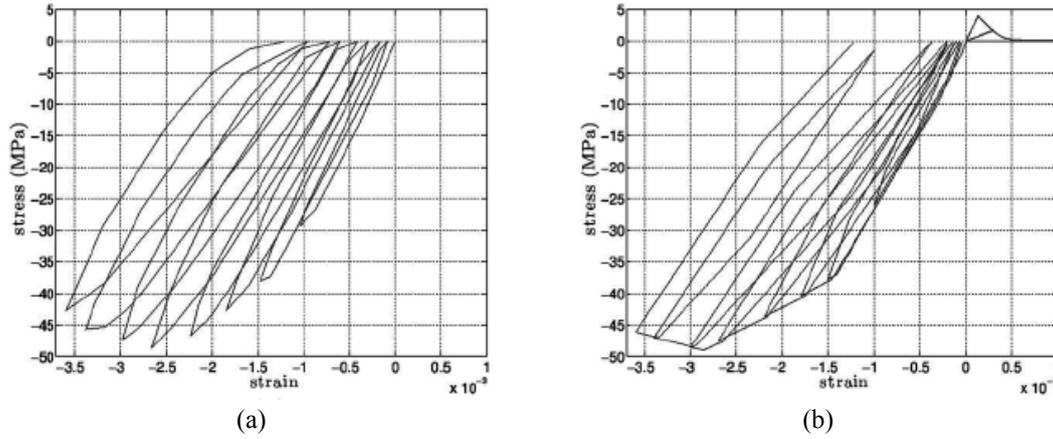
Fig. 5 Hysteresis loops for concrete specimen in compression under cyclic loading: a) left – experimental results (Ramtani 1990) b) modeling with coupled plasticity-damage-viscosity model with linear evolution equations for internal variables

Table 1 Set of internal variables α, corresponding conjugate variables A and corresponding moduli jointly denoted as PC (parameters constants)

	t/c		Compression					Tension		
α	$\bar{\epsilon}^v$	$\bar{\epsilon}^p$	$\bar{\xi}^p$	$\bar{\lambda}^p$	$\bar{D}$	$\bar{\xi}^d$	$\bar{\bar{u}}^d$	$\bar{\bar{\xi}}^p$	$\bar{\bar{D}}$	$\bar{\bar{\xi}}^d$
A	σ^v	σ	$\bar{q}^p$	$\bar{\kappa}^p$	$\dfrac{\sigma^2}{2}$	q^d	t	$\bar{\bar{q}}^p$	$\dfrac{t^2}{2}$	$\bar{\bar{q}}^d$
PC	E, η	$\bar{E}$	$\bar{K}^p$	$\bar{H}^p$	$\bar{E}^{-1}$	$\bar{K}^d$	$\bar{\bar{E}}$	$\bar{\bar{K}}^p$	$\bar{\bar{E}}^{-1}$	σ_∞, α

hysteresis loop indeed is.

More, precisely, for describing the cyclic response of concrete in compression we would need the whole list of internal variables: $\bar{\varepsilon}^v$ and $\bar{\varepsilon}^p$ as the viscous and plastic deformations, $\bar{\xi}^p$ and $\bar{\lambda}^p$ as strain-like variables that represent isotropic and kinematic plastic hardening, $\bar{D}$ as the damage compliance quantifying the reduction in elastic modulus and $\bar{\xi}^d$ as the strain-like isotropic hardening for damage. Furthermore, in the final failure stage with softening response where the stress decreases for increasing strain, we need additional internal variables: up as localized plastic deformation, $\bar{\bar{\xi}}^p$ as measure of plastic strain softening in compression, as well as $\bar{\bar{D}}$ as the damage softening compliance and $\bar{\bar{\xi}}^d$ as measure of damage strain softening in tension. In order to place these developments in the sound thermodynamics framework (Ibrahimbegovic 2009), each of these strain-like internal variables has associated stress-like thermodynamically conjugate variables and corresponding moduli connecting two sets of conjugate variable with constant values, which chosen for computational efficiency. Table 1, given below, summarizes the full set of internal variables, their conjugate variables in the sense of thermodynamics (Ibrahimbegovic 2009), and corresponding moduli.

The set of internal variables in Table 1 above, along with the total strain ε can be used to define the total energy of the system, by assuming additive split of total deformation along with corresponding additive split of different mechanisms contributions

$$
\begin{aligned}
\psi^+(u,\boldsymbol{\alpha}) &= \bar{\psi}^e(\bar{u}^+) + \left(\bar{\bar{\psi}}^d(\bar{u}^+,\bar{\bar{D}}) + \bar{\bar{\Xi}}^d(\bar{\bar{\xi}}^d)\right)\delta_{\bar{x}} \\
\psi^-(u,\boldsymbol{\alpha}) &= \bar{\psi}^d(\bar{u}^-,\bar{\epsilon}^p,\bar{D}) + \bar{\Xi}^p(\bar{\xi}^p) + \bar{\Lambda}^p(\bar{\lambda}^p) + \bar{\Xi}^d(\bar{\xi}^d) + \\
&\quad \left(\bar{\bar{\psi}}^e(\bar{u}^-,\bar{u}^p) + \bar{\bar{\Xi}}^p(\bar{\bar{\xi}}^p)\right)\delta_{\bar{x}}
\end{aligned}
\tag{5}
$$

where the top row summarized the energy in tension, as combination of elastic energy and damage softening in tension, whereas the second row presents the energy in compression as combination of elastic energy with viscosity, the plastic hardening potentials, both isotropic and kinematic, the damage hardening potential, and finally the plastic softening potentials.

The total energy dissipation that takes into account all different sources of energy dissipation can then be explicitly written as combination of viscous, plastic and damage dissipations, including both hardening and softening response phase

$$
\begin{aligned}
\dot{\mathcal{D}} &= \underbrace{\sigma^v\dot{\bar{\epsilon}}^v}_{\dot{\mathcal{D}}^v} + \underbrace{\sigma\dot{\bar{\epsilon}}^p + \bar{q}^p\dot{\bar{\xi}}^p + \bar{\kappa}^p\dot{\bar{\lambda}}^p}_{\dot{\mathcal{D}}^p} + \underbrace{\frac{1}{2}\sigma\dot{\bar{D}}\sigma + \bar{q}^p\dot{\bar{\xi}}^d}_{\dot{\mathcal{D}}^d} + \\
&\quad \underbrace{\left(\mathsf{t}\dot{\bar{u}}^p + \bar{q}^p\dot{\bar{\xi}}^p\right)\delta_{\bar{x}}}_{\dot{\bar{\mathcal{D}}}^p} + \underbrace{\left(\frac{1}{2}\mathsf{t}\dot{\bar{\bar{D}}}\mathsf{t} + \bar{q}^d\dot{\bar{\bar{\xi}}}^d\right)\delta_{\bar{x}}}_{\dot{\bar{\mathcal{D}}}^d}
\end{aligned}
\tag{6}
$$

The activation of each particular internal variable is monitored through corresponding yield or damage function. In particular, for internal variables in compression with $\sigma<0$ we use, in order, viscosity activation criterion, plasticity criterion, damage criterion and softening plasticity criterion

$$
\begin{aligned}
\bar{\phi}^{v,-}(\sigma) &= -\sigma^v = -\left(\sigma - \sigma^d\right) \leq 0 \\
\bar{\phi}^{p,-}(\sigma,\bar{q}^p,\bar{\kappa}^p) &= |\sigma + \bar{\kappa}^p| - (\sigma_y - \bar{q}^p) \leq 0 \\
\bar{\phi}^{d,-}(\sigma,\bar{q}^d) &= -\sigma - (\sigma_f - \bar{q}^d) \leq 0 \\
\bar{\bar{\phi}}^{p,-}(\mathsf{t},\bar{q}^p) &= -\mathsf{t} - (\sigma_u^c - \bar{q}^p) \leq 0
\end{aligned}
\tag{7}
$$

Similarly, for internal variables in tension with $\sigma>0$ we use viscosity activation criterion and damage softening criterion

$$
\begin{aligned}
\bar{\phi}^{v,+}(\sigma) &= \sigma^v = \sigma - \sigma^e \leq 0 \\
\bar{\bar{\phi}}^{d,+}(\mathsf{t},\bar{q}^d) &= \mathsf{t} - (\sigma_u^t - \bar{\bar{q}}^d) \leq 0
\end{aligned}
\tag{8}
$$

The evolution equations of internal variables can then be obtained by appealing to the principle of maximum plastic dissipation which should be applied for inelastic criteria in (7) and (8) above that take zero value; we thus obtain the evolution equations for viscous strain, plastic strain and damage compliance, along with corresponding hardening and softening variables in compression and in tension. More precisely, the complete list of evolution equations can be presented as follows:

Viscosity

$$
\dot{\bar{\epsilon}}^v = \frac{\bar{\phi}^v}{\eta}\frac{\partial\bar{\phi}^v}{\partial\sigma}, \frac{\bar{\phi}^v}{\eta} = \dot{\bar{\gamma}}^v \qquad\qquad \gamma \geq 0, \phi^{\dot{v}} \leq 0, \dot{\gamma}^v\phi^v = 0
$$

Continuous plasticity

$$\dot{\epsilon}^{\mathrm{p}} = \dot{\gamma}^{\mathrm{p}} \frac{\partial \phi^{\mathrm{p}}}{\partial \sigma}$$

$$\dot{\xi}^{\mathrm{p}} = \dot{\gamma}^{\mathrm{p}} \frac{\partial \phi^{\mathrm{p}}}{\partial q^{\mathrm{p}}}$$

$$\dot{\lambda}^{\mathrm{p}} = \dot{\gamma}^{\mathrm{p}} \frac{\partial \phi^{\mathrm{p}}}{\partial k^{\mathrm{p}}}$$

$$\dot{\gamma}^{\mathrm{p}} \geq 0, \ \phi^{\mathrm{p}} \leq 0, \ \dot{\gamma}^{\mathrm{p}} \phi^{\mathrm{p}} = 0$$

Discrete plasticity

$$\dot{\bar{\bar{u}}}_{i}^{\mathrm{p}} = \dot{\bar{\bar{\gamma}}}_{i}^{P} \frac{\partial \bar{\bar{\phi}}_{i}^{P}}{\partial \bar{\bar{t}}_{i}^{P}}$$

$$\dot{\bar{\bar{\xi}}}_{i}^{\mathrm{p}} = \dot{\bar{\bar{\gamma}}}_{i}^{P} \frac{\partial \bar{\bar{\phi}}_{i}^{P}}{\partial \bar{\bar{q}}_{i}^{P}}$$

$$\dot{\bar{\bar{\gamma}}}_{i}^{P} \geq 0, \ \phi_{i}^{P} \leq 0, \ \dot{\bar{\bar{\gamma}}}_{i}^{P} \bar{\bar{\phi}}_{i}^{P} = 0$$

Continuous damage

$$\dot{D}\sigma = \dot{\gamma}^{\mathrm{d}} \frac{\partial \phi^{\mathrm{d}}}{\partial \sigma}$$

$$\dot{\xi}^{\mathrm{d}} = \dot{\gamma}^{\mathrm{d}} \frac{\partial \phi^{\mathrm{d}}}{\partial q^{\mathrm{d}}}$$

$$\dot{\gamma}^{\mathrm{p}} \geq 0, \ \phi^{\mathrm{p}} \leq 0, \ \dot{\gamma}^{\mathrm{p}} \phi^{\mathrm{p}} = 0 \tag{9}$$

Discrete damage

$$\dot{\bar{\bar{D}}}_{i}t_{i} = \dot{\bar{\bar{\gamma}}}_{i}^{\mathrm{d}} \frac{\partial \bar{\bar{\phi}}_{i}^{\mathrm{d}}}{\partial t_{i}}$$

$$\dot{\bar{\bar{\xi}}}_{i}^{\mathrm{d}} = \dot{\bar{\bar{\gamma}}}_{i}^{\mathrm{d}} \frac{\partial \bar{\bar{\phi}}_{i}^{\mathrm{d}}}{\partial \bar{\bar{q}}_{i}^{\mathrm{d}}}$$

$$\dot{\bar{\bar{\gamma}}}_{i}^{\mathrm{d}} \geq 0, \ \bar{\bar{\phi}}_{i}^{\mathrm{d}} \leq 0, \ \dot{\bar{\bar{\gamma}}}_{i}^{\mathrm{d}} \bar{\bar{\phi}}_{i}^{\mathrm{d}} = 0$$

In a very similarmanner one can provide the corresponding set of internal variables and corresponding evolution equations for many other sources of energy dissipation, such as with soils (Hadzalic *et al*. 2018a, b, c, Hadzalic *et al*. 2019, Hadzalic *et al*. 2020, Saksala 2015, Saksala 2016, Saksala 2020), massive concrete structures (Karavelic *et al*. 2019, Rukavina *et al*. 2019, Hautefeuille *et al*. 2009), reinforced concrete structures (Ibrahimbegovic *et al*. 2010), steel structures (Imamovic *et al*. 2015, Imamovic *et al*. 2018, Nguyen *et al*. 2021), or structures controlled by frictional device (Mejia Nava *et al*. 2020).

This completely defines the computations at material-scales that allows providing the intrinsic description of sources of energy dissipation.

2.2 Structure-scales hybrid-stress variational formulation granting computational efficiency

In this section we complete development that pertain to structure-scales. To that end, we choose the multi-fiber 3D beam model of Euler-Bernoulli type, which is very suitable for modeling many frame structures (see Fig. 6).

Each fiber structural-level response is considered fully described by usual Euler-Bernoulli beam kinematics featuring the displacement at the neutral axis along the beam axis and derivative of transverse displacement that is in agreement with the hypothesis that the beam cross-sections remain plane after deformation and also remain perpendicular to the deformed neutral axis of the beam. If in addition we include the possible failure within the fiber, with u^f as the failure mode, we can write the fiber kinematics according to
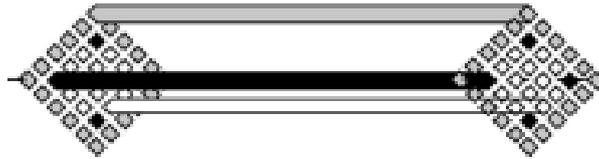
Fig. 6 Multi-scale 3D beam structural model with fiber-type of micro-structure

$$u^f(x,t) = \underbrace{\tilde{u}(x,t) - z^f \frac{\partial \tilde{w}(x,t)}{\partial x}}_{\tilde{u}^f(x,t)} + \sum_{i=1}^{n_{dis}} \left(\mathcal{H}_{\Gamma_i}(x) - \varphi_i^f(x) \right) \bar{\bar{u}}_i^f(t)$$

(10)

where z^f is the distance of a particular fiber to neutral axis, H_Γ is the Heaviside function (e.g., Clough and Penzien 2006) introducing crack-like opening in beam kinematics, and φ^f is the attenuation function that removes the influence of crack from distant displacement filed (e.g., see Ibrahimbegovic 2009).

We next set the weak form of equations of motions by using the hybrid-stress variational formulation (Ibrahimbegovic 2009) at the beam structural level, and split the integrals over the beam cross and beam length. The former can then be simplified to summing up over total number of fibers within the beam cross-section, leading to the final expression

$$\sum_f A^f \int_L \left(\rho \frac{\partial^2 \tilde{u}}{\partial t^2} \delta \tilde{u} + \frac{\partial \delta \tilde{u}}{\partial x} \sigma^f \right) dx - \delta U^{ext} = 0$$

$$\int_L \delta \sigma^f \left(\frac{\partial \tilde{u}}{\partial x} - \bar{\epsilon}^v - \bar{\epsilon}^p - \bar{\bar{u}}^p \frac{d\varphi_i}{dx} \right) dx = 0 \quad \forall f$$

$$\dot{\gamma}^v \geq 0 , \; \phi^v \leq 0 , \; \dot{\gamma}^v \phi^v = 0 \quad \forall \mathbf{x}$$

$$\dot{\gamma}^p \geq 0 , \; \phi^p \leq 0 , \; \dot{\gamma}^p \phi^p = 0 \quad \forall \mathbf{x}$$

$$\dot{\gamma}^d \geq 0 , \; \phi^d \leq 0 , \; \dot{\gamma}^d \phi^d = 0 \quad \forall \mathbf{x}$$

$$\dot{\bar{\bar{\gamma}}}^p \geq 0 , \; \bar{\bar{\phi}}^p \leq 0 , \; \dot{\bar{\bar{\gamma}}}^p \bar{\bar{\phi}}^p = 0$$

(11)

We note that the hybrid-stress formulation considers the stress as independent field, so that we have to provide not only usual finite element interpolations for displacement field (e.g., Ibrahimbegovic 2009), but also for stress. The former is selected by using the standard Hermite polynomials (Clough and Penzien 2006) in agreement with the chosen Euler-Bernoulli beam kinematics

$$\tilde{u}^h(\mathbf{x}, t)|_{\mathbf{x} \in \Omega^e} = \mathbf{N}(\mathbf{x}) \mathbf{d}^e(t)$$

(12)

Such choice of discrete approximation implies continuity of displacement field and its derivatives (for transverse component) from one element to another. By replacing these interpolations into the weak form in (11) above, we recover the semi-discrete format of equations of motion, with time dependent terms regrouping the inertia forces, internal and external force.

$$\underbrace{\overset{n_{el}}{\underset{e=1}{A}} \mathbf{M}^e \; \ddot{\mathbf{d}}_{n+1}^e}_{\text{inertial forces}} + \underbrace{\overset{n_{el}}{\underset{e=1}{A}} \mathbf{f}_{n+1}^{int,e}}_{\text{internal forces}} \underbrace{- \int_{\Omega^e} \mathbf{N}^T \mathbf{b}_{n+1} d\Omega^e - \int_{\partial\Omega^e} \mathbf{N}^T \bar{\mathbf{t}}_{n+1} dS^e}_{\text{external forces}} = \mathbf{0}$$

(13)

The internal force has to be computed from the stress within each fiber as indicated in $(11)_2$. Now, the hybrid-stress formulation comes to rescue, for it provides the stress interpolation chosen independently in each element fiber, since no stress field continuity is required in the hybrid-stress weak form; thus, we can write

$$\sigma^{f,h}(x,t)|_{\mathbf{x} \in \Omega^e} = \mathbf{S}(x) \beta^f(t)$$

(14)

which allows to obtain the internal force very easily by summing up stresses in each particular fiber.

Needless to say, the set of semi-discrete equations of motion in (13) above is highly non-linear. Thus, we have to perform incremental-iterative procedure in order to advance the solution in time (e.g., see Ibrahimbegovic 2009). The hybrid-stress variational formulation again comes to a rescue, in that it allows not to compute the tangent stiffness matrix, but rather its inverse. The main advantage of such approach is in the fact that all contributions form different energy dissipation mechanisms remain fully uncoupled and we can account for all their contributions in a simple additive manner. More precisely, by linearizing $(11)_2$ we can obtain the inverse of the tangent compliance matrix, which can be inverted to obtain the corresponding tangent stiffness matrix. This can be written as follows

$$\begin{pmatrix} c_t\mathbf{M}^e & \mathbf{G}^e \\ \mathbf{G}^{e,T} & -\hat{H} \end{pmatrix} \left\{ \begin{array}{c} \mathbf{d}_{n+1}^{(i)} \\ \beta_{n+1} \end{array} \right\} = \left\{ \begin{array}{c} \mathbf{R}_{d,n+1}^{(i)} \\ 0 \end{array} \right\}$$

$$\Rightarrow \mathbf{K}^{e,tan(i)} = c_t\mathbf{M}^e + \mathbf{G}^e\hat{H}^{-1}\mathbf{G}^{eT}$$

$$\hat{H}_{n+1} = H_n + \underbrace{\left(\bar{K}^p\right)^{-1}L}_{\text{si } \bar{\gamma}_{n+1}^p > 0} + \underbrace{\left(\bar{K}^d\right)^{-1}L}_{\text{si } \bar{\gamma}_{n+1}^d > 0} + \underbrace{\left(\bar{\bar{K}}^p\right)^{-1}}_{\text{si } \bar{\bar{\gamma}}_{n+1}^p > 0} \tag{15}$$

$$H_n = \frac{\Delta t \bar{D}_n(x_1)}{\tau + \Delta t} L$$

which fully explains the structure-scale computations.

We note in passing that two key ingredients that grant very high computational efficiency of the proposed approach are: i) hybrid-stress formulation that allows to reduce the problem to computing the elasto-visco-plastic-damage compliance, where different mechanisms remain additively coupled so that the contribution of each one can be computed independently; ii) the linear hardening/softening laws that allow to avoid the local iterative procedure at the level of internal variable evolution, resulting in approximate representation of hysteresis loop shape but correct representation of the enclosed area.

3. Results of numerical simulations in cyclic loading

3.1 Material-scales identification procedure with judicious choice of loading program

The main advantage of the proposed approach for damping mechanism identification is in intrinsic value, with parameters that can be identified at the material scale. In particular, in this example we provide an illustrative procedure for such identification related to cyclic response of concrete in compression. The experimental results of (Ramtani 1990) show the great complexity of such response, as illustrated in Fig. 7(a), with degradation of elastic response from cycle to cycle due to damage, with permanent plastic deformation and sort of rounded shape of hysteresis loops. The proposed model with linear hardening/softening evolution equations can capture the salient features, but not such a rounded shape of each hysteresis loop. Rather, the hysteresis loops produced by proposed model are of sharp contours, which does not allow to match the real rounded shape of
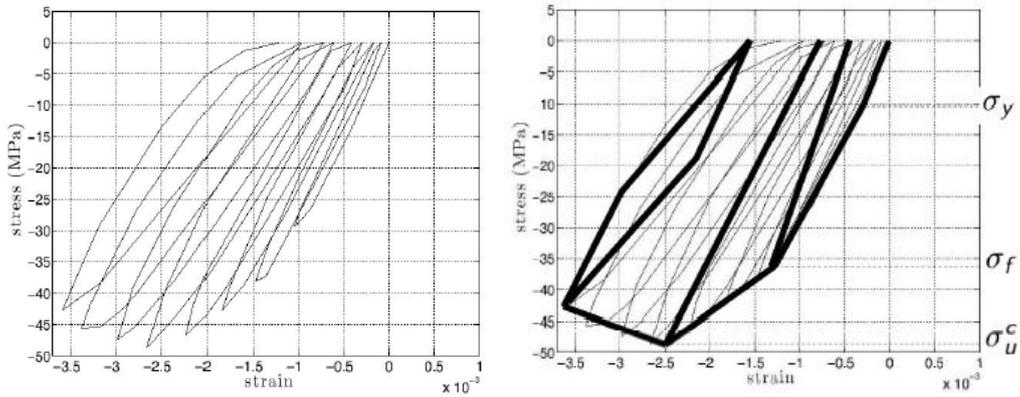
Fig. 7 Hysteresis loops for concrete specimen in compression under dynamic cyclic loading: i) left – experimental results ii) modeling with coupled plasticity-damage-viscosity model with linear evolution equations for internal variables

(a)

(b)

(c)

(d)
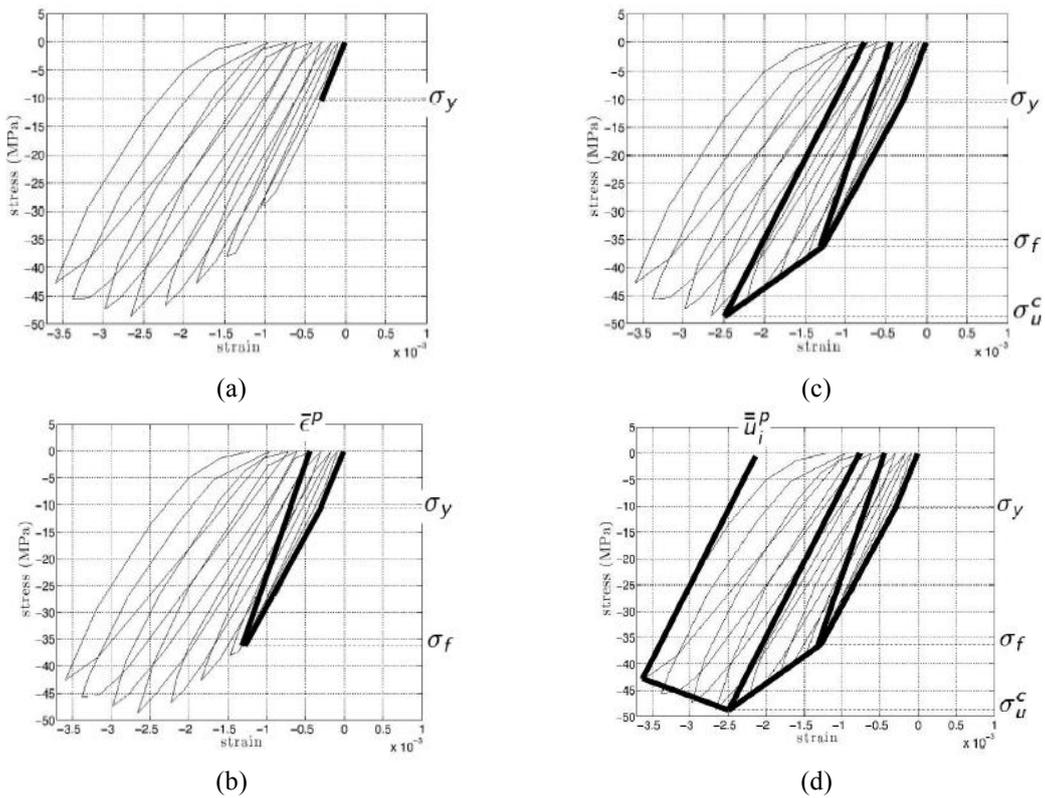
Fig. 8 Full identification process for different model parameters with coupled viscosity-plasticity-damage with hardening and softening along with dedicated loading program to split identification into separate stages

experimentally obtained hysteresis loops. Yet, what we seek to match is not the shape, but rather the area enclosed by each hysteresis loop, which corresponds to total dissipation in each loop. Hence,

the basis of material scales identification is indeed dissipation base, which is already proved to be the most judicious choice (e.g., Ibrahimbegovic *et al.* 2021).

The parameter identification of coupled viscosity – plasticity – damage model with hardening/ softening, is further illustrated in Fig. 8. Namely, the key idea is to choose the most appropriate loading program, which will favor the dominant contribution of a particular model component. Thus, it becomes easier to isolate the main contribution and identify the corresponding value of the model parameter. In particular, in Fig. 8(a), we can start by identifying the yield stress value. Then, by using loading-unloading program, we can further identify the damage stress, as shown in Fig. 8(b). Furthermore, we can push the response towards ultimate stress to identify the highest possible value of stress, as illustrated in Fig. 8(c). Finally, we can carry on with a loading-unloading cycle in softening in order to identify the corresponding amount of dissipation in softening, as shown in Fig. 8(d), (c).

3.2 Typical earthquake vibration response and amplitude decay

The parameter identification procedure, discussed in previous example, is carried out for simple proportional loading. In reality, the model performance should finally be evaluated with respect to real-life loading applications, such as typical earthquake vibration response. In Fig. 9 we illustrate a typical earthquake ground acceleration record, which when multiplied with so-called directional mass (e.g., see Clough and Penzien 2006) amounts to equivalent external force.

Several typical response records for such an earthquake loading are further illustrated in Fig. 10. In particular, we consider the response in displacement, total force and stress records at particular location, with both the one that enters and the other that does not reach the softening phase. We can see that with the typical resolution of such records, we are much less concerned with rounded or not rounded shape of typical hysteresis loop. What is more important is the total area of each hysteresis loop with corresponding amount of dissipation. For that, the proposed model can ensure sufficiently good performance.

3.3 Structure heterogeneities influence on vibration amplitude decay

In this last example, we connect the material-scale and structural-scale behavior. In particular, we consider the vibrations of a cantilever beam, which implements the proposed coupled visco-
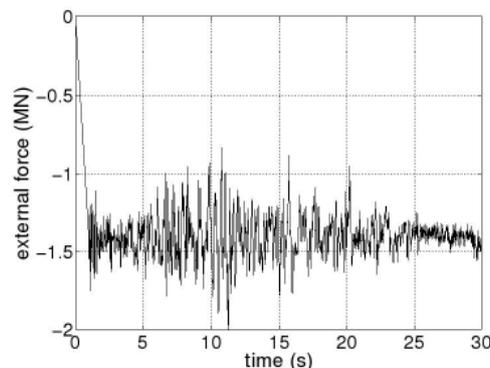
Fig. 9 Typical earthquake ground acceleration time history
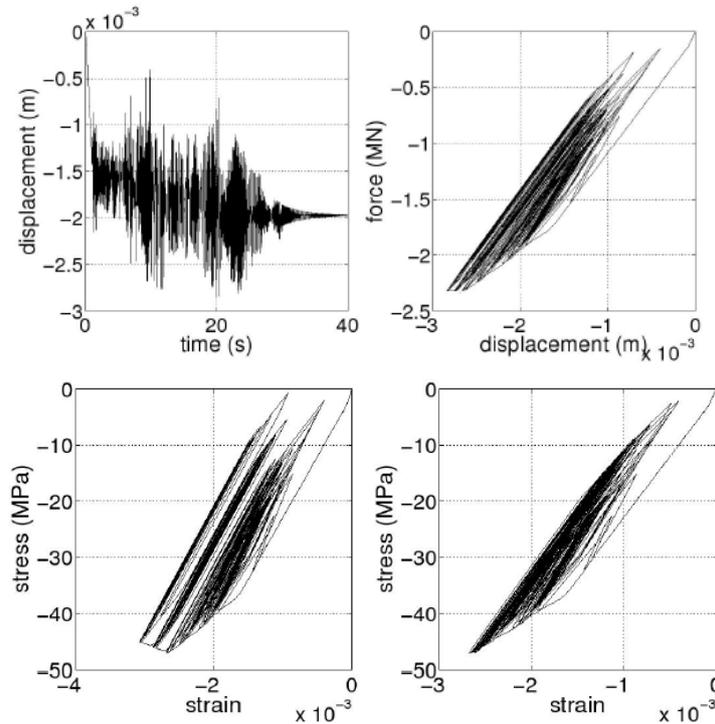
Fig. 10 Typical hystersis loops under earthquake ground acceleration time history

(a)

(b)
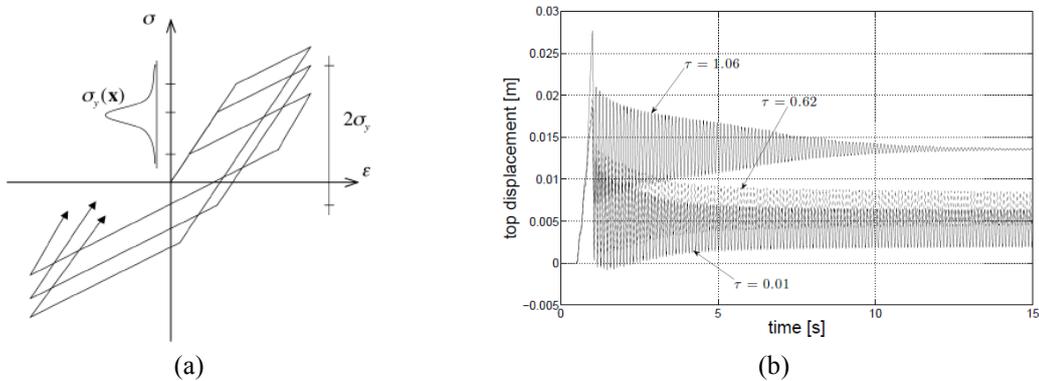
Fig. 11 Typical amplitude decay with coupled plasticity-damage-viscosity model with: i) linear amplitude decay for fricton-like dissipation (Inman 2001) for homogeneous structure versus exponential amplitude decay for heterogeneous structure (with τ quantifying standard deviation in yield stress $\phi(\sigma, \kappa) = |\sigma + \kappa| - f_0(x)\sigma_y$

plastic-damage model. The key novelty is to allow for structural-scale heterogeneities, which implies that the material parameters are not constant, but vary along the beam. In particular, such variation is modeled by using the chosen probability distribution of the yield stress of the plastic component of our model, where the simple Gaussian distribution is chosen. Hence, the large contribution of structure heterogeneities is characterized by large standard deviation of the yield stress; see Fig.

11(a), whereas a small value of the standard deviation implies that the structure is considered homogeneous.

The results we thus obtain in Fig. 11(b) are truly remarkable. Namely, for small standard deviation of the yield stress and homogeneous structure, we indeed obtain linear decay in vibration amplitudes, typical of friction-like resistance as shown in (Inman 2001). This is not surprising given equivalence between phenomena of friction and plasticity (e.g., Ibrahimbegovic 2009).

However, for heterogeneous structure for which large value of standard deviation of the yield stress is present, the decay of vibration amplitude becomes exponential, just as often observed in experiments. The result is indeed very valuable for it allows combining the intrinsic material-scales parameter identification of energy dissipation mechanisms with structure-scale heterogeneities in order to recover experimentally observed results.

5. Conclusions

The main challenge we successfully tackled in this paper is the development of a damping model to accurately predict vibration amplitude reduction for very different loading programs and any size of structure. The main idea to combine the material-scale for intrinsic interpretation of energy dissipation mechanism and structure-scale to account for heterogeneities, which is all consistently placed within the framework of multi-scale analysis. The proposed approach thus unifies the know-how of material-science, where different sources of energy dissipation at captured at material-scales via so-called representative volume element; see accompany paper (Mejia *et al*. 2021), and structural –scale where the structure heterogeneities are playing the crucial role in providing the realistic bounds within the framework of stochastic analysis (Ibrahimbegovic *et al*. 2021).

The proposed approach is definitely more costly than using the classical Rayleigh damping. Namely, we have illustrated details for concrete structures, where one needs different failure mechanisms like plasticity, damage and viscosity to represent different sources of dissipation are reproduce the typical hysteresis loops of concrete with both residual deformation and change of initial elastic response. However, the computational efficiency of such an approach was still possible to achieve thanks to two key ingredients: i) hybrid-stress variational formulation that allows to directly compute visco-plastic-damage compliance where the contributions of different energy dissipation mechanisms remains additive and can be computed independently, and ii) linear hardening/softening laws that allow to avoid local iterative procedure and can still well approximate the total area of each hysteresis loop and corresponding amount of energy dissipation.

The most remarkable results of the proposed approach is in its ability to recover the exponential amplitude decay, by accounting for structure heterogeneities and by allowing for variability of elasticity limit. Such exponential amplitude decay is typical of many experimental results, which justified use of Rayleigh damping as the most appropriate damping model for structures. However, contrary to Rayleigh damping calibration that can be done only for a chosen frequency and on a single structure, the proposed approach can be adapted to any structure size and full interval of frequencies of interest. The price to pay is in terms of multi-scale nonlinear analysis, which as shown herein can still be rendered quite efficient.

The details illustrated in this paper for cyclic concrete model can be easily adapted to other materials, such as soils (Hadzalic *et al*. 2018a, b, c, Hadzalic *et al*. 2019, Hadzalic *et al*. 2020, Saksala 2015, Saksala 2016, Saksala 2020), massive concrete structures (Karavelic *et al*. 2019, Rukavina *et al*. 2019, Hautefeuille *et al*. 2009), reinforced concrete structures (Ibrahimbegovic *et*

al. 2010), steel structures (Imamovic *et al.* 2015, Imamovic *et al.* 2018, Nguyen *et al.* 2021), or structures controlled by frictional device (Mejia Nava *et al.* 2020).

Acknowledgments

References

Chopra, A. (1995), *Dynamics of Structures: Theory and Applications to Earthquake Engineering*, Prentice Hall.

Clough, R.W. and Penzien, J. (2006), *Dynamics of Structures*, McGraw-Hill.

Do, X.N. and Ibrahimbegovic, A. (2018), "2D continuum viscodamage-embedded discontinuity model with second order mid-point scheme", *Coupl. Syst. Mech.*, **7**, 669-690. http://doi.org/10.12989/csm.2018.7.6.669.

Geradin, M. and Rixen, D. (2015), *Mechanical Vibrations: Theory and Applications to Structural Dynamics*, Wiley.

Hadzalic E., Ibrahimbegovic, A. and Nikolic, M. (2018), "Failure mechanisms in coupled poro-plastic medium", *Coupl. Syst. Mech.*, **7**, 43-59. http://doi.org/10.12989/csm.2018.7.1.043.

Hadzalic, E., Ibrahimbegovic, A. and Dolarevic, S. (2018), "Failure mechanisms in coupled soil-foundation systems", *Coupl. Syst. Mech.*, **7**, 27-42. http://doi.org/10.12989/csm.2018.7.1.027.

Hadzalic, E., Ibrahimbegovic, A. and Dolarevic, S. (2018), "Fluid-structure interaction system predicting both internal pore pressure and outside hydrodynamic pressure", *Coupl. Syst. Mech.*, **7**, 659-668. http://doi.org/10.12989/csm.2018.7.6.669.

Hadzalic, E., Ibrahimbegovic, A. and Dolarevic, S. (2019), "Acoustic fluid-structure interaction with structure built of saturated porous media capable of predicting localized failure with cracks", *Comput. Struct.*, **214**, 73-93.

Hadzalic, E., Ibrahimbegovic, A. and Dolarevic, S. (2020), "3D thermo-hydro-mechanical coupled discrete beam lattice model of saturated poro-plastic medium", *Coupl. Syst. Mech.*, **9**, 125-145. http://doi.org/10.12989/csm.2020.9.2.125.

Hautefeuille, M., Melnyk, S., Colliat, J.B. and Ibrahimbegovic, A. (2009), "Probabilistic aspects of localized failure of massive heterogeneous structures", *Int. J. Eng. Comput.*, **26**, 166-184.

Ibrahimbegovic A. and Ademovic, N. (2019), *Nonlinear Dynamics of Structures Under Extreme Transient Loads*, CRC Press.

Ibrahimbegovic, A. (2009), *Nonlinear Solid Mechanics: Theoretical Formulations and Finite Element Solution Methods*, Springer, Berlin.

Ibrahimbegovic, A. (2016), *Computational Methods for Solids and Fluids: Multiscale Analysis, Probability Aspects and Model Reduction*, Springer.

Ibrahimbegovic, A., Boulkertous, A., Davenne, L. and Brancherie, D. (2010), "Modeling of reinforced-concrete structures providing crack-spacing based on XFEM, ED-FEM and novel operator split solution procedure", *Int. J. Numer. Meth. Eng.*, **83**, 452-481. https://doi.org/10.1002/nme.2838.

Ibrahimbegovic, A., Colliat, J.B., Hautefeuille, M., Brancherie, D. and Melnyk, S. (2011), "Probability based size effect representation for failure of civil engineering structures built of heterogeneous materials", *Computational Methods in Stochastic Dynamics*, Eds. M. Papadrakakis, M. Fragiadakis, G. Stefanou, Springer, Berlin.

Ibrahimbegovic, A., Davenne, L., Markovic, D. and Dominguez, N. (2014), "Performance based earthquake-

resistant design: Migrating towards nonlinear models and probabilistic framework", *Performance Based Seismic Engineering – Vision for Earthquake Resilient Society*, Ed. M. Fischinger Springer.

Ibrahimbegovic, A., Jehel, P. and Davenne, L. (2008), "Coupled damage-plasticity constitutive model and direct stress interpolation", *Comput. Mech.*, **42**, 1-11. https://doi.org/10.1007/s00466-007-0230-6.

Ibrahimbegovic, A., Matthies, H.G. and Karavelic, E. (2021), "Reduced model of macro-scale stochastic plasticity identification by Bayesian inference in application to quasi-brittle failure of concrete", *Compot. Meth. Appl. Mech. Eng.*, **372**, 113428. https://doi.org/10.1016/j.cma.2020.113428.

Imamovic, I., Ibrahimbegovic, A. and Mesic, E. (2018), "Coupled testing-modeling approach to ulitmate state computation of steel structures with connections for statics and dynamics", *Coupl. Syst. Mech.*, **7**, 555-581. http://doi.org/10.12989/csm.2018.7.5.555.

Imamovic, I., Ibrahimbegovic, A., Knopf-Lenoir, C. and Mesic, E. (2015), "Plasticity-damage model parameters identification for structural connections", *Coupl. Syst. Mech.*, **4**, 337-364. http://doi.org/10.12989/csm.2015.4.4.337.

Inman, D.J. (2001), *Engineering Vibrations*, Prentice Hall Inc.

Jehel, P., Davenne, L., Ibrahimbegovic, A. and Leger, P. (2010), "Towards robust viscoelastic-plastic-damage model with different hardening-softening capable of representing salient phenomena in seismic loading applications", *Comput. Concrete*, **7**(4), 365-386. http://doi.org/10.12989/cac.2010.7.4.365.

Karavelic, E., Ibrahimbegovic, A. and Dolarevic, S. (2019), "Multi-surface plasticity model for concrete with 3D hardening/softening failure modes for tension, compression and shear", *Comput. Struct.*, **221**, 74-90. https://doi.org/10.1016/j.compstruc.2019.05.009.

Karavelic, E., Nikolic, M., Ibrahimbegovic, A. and Kurtovic, A. (2019), "Concrete meso-scale model with full set of 3D failure modes with random distribution of aggregate and cement phase. Part I: Formulation and numerical implementation", *Comput. Meth. Appl. Mech. Eng.*, **344**, 1051-1072. https://doi.org/10.1016/j.cma.2017.09.013.

Kožar, I., Ibrahimbegovic, A. and Rukavina, T. (2018), "Material model for load rate sensitivity", *Coupl. Syst. Mech.*, **7**, 141-162. http://doi.org/10.12989/csm.2018.7.2.141.

Mejia Nava, R.A., Ibrahimbegovic, A. and Lozano, R. (2020), "Instability phenomena and their control in statics and dynamics: Application to deep and shallow truss and frame structures", *Coupl. Syst. Mech.*, **9**, 47-62. http://doi.org/10.12989/csm.2020.9.1.047.

Mejia Nava, R.A., Ibrahimbegovic, A., Dominguez-Ramirez, N. and Flores-Mendez, E. (2021), "Viscoelastic behaviour of concrete structures subject to earthquake", *Coupl. Syst. Mech.*, **10**, (in Press)

Nguyen, C.U. and Ibrahimbegovic, A. (2021), "Hybrid-stress triangular finite element with enhanced performance for statics and dynamics", *Comput. Meth, Appl. Mech. Eng.*, **372**, 113381. https://doi.org/10.1016/j.cma.2020.113381.

Ramtani, S. (1990), "Contribution to the modeling of the multi-axial behavior of damaged concrete with description of the unilateral characteristics", PhD Thesis, Paris 6 University. (in French)

Rukavina, I., Ibrahimbegovic, A., Do, X.N. and Markovic, D. (2019), "ED-FEM multi-scale computation procedure for localized failure", *Coupl. Syst. Mech.*, **8**, 117-127. http://dx.doi.org/10.12989/csm.2019.8.2.117.

Saksala, T. and Ibrahimbegovic, A. (2020), "Thermal shock weakening of granite rock under dynamic loading: 3D numerical modelling based on embedded discontinuity finite elements", *Int. J. Numer. Anal. Meth. Geomech.*, **44**, 1788-1811. https://doi.org/10.1002/nag.3107.

Saksala, T., Brancherie, D. and Ibrahimbegovic, A. (2016), "Numerical modeling of dynamic rock fracture with a combined 3D continuum viscodamage-embedded discontinuity model", *Int. J. Numer. Anal. Meth. Geomech.*, **40**, 1339-1357. https://doi.org/10.1002/nag.2492.

Saksala, T., Brancherie, D., Harari, I. and Ibrahimbegovic, A. (2015), "Rate-dependent continuum damage-embedded discontinuity model for explicit dynamic analyses of fracture in quasi-brittle materials", *Int. J. Numer. Meth. Eng.*, **101**, 230-250.